Master Thesis

Simulations and measurements of InGaAlP LEDs

Björn Jönsson

Division for Solid State Physics
Faculty of Engineering

LUND UNIVERSITY

SWEDISH ICT ACREO

Abstract

This work concerns the light extraction from InGaAlP LEDs. Two possible improvements are studied. Resonant cavity LEDs with a long cavity (optical path $\gg \lambda$) are simulated and improvements in light output are found, but with possibly unwanted effects, such as the spectrum splitting into different peaks at different wavelengths, on the emission pattern. Also, measurements are done on four different top electrode geometries, which are ranked with respect to light output. Grid-shaped electrodes are shown to outperform more concentrated designs.

Acknowledgments

First, I would like to thank my supervisors, Dr. Qin Wang and Dr. Ingemar Petermann, for giving me the opportunity to do this work.

The electrode fabrication described in chapter 4 was done by Susanne Almquist who also instructed me in lab procedure

My friends Björn and Elena let me stay at their place will I was looking for a place to live in Stockholm. For that I am grateful.

I would also like to thank everybody at Acreo for companionsship, help and banter during this period.

Contents

Chapter 1

Introduction

Figure 1.1: An example of LED use: a Christmas tree decorated with LED lights.

Light emitting diodes (LEDs) are found everywhere. They are used as indicator lights and in displays, for backlighting screens, in communications and increasingly for both general illumination and decorative lightning. Using different materials systems, the entire visible spectrum is available, and also IR and UV. Appealing properties of LEDs are small size, a high reliability, and most importantly, a high efficiency. For certain applications, e.g communications, the low spectral width is another plus.

One large problem with making efficient LEDs is the extraction of the generated light from the LED chip. The high refractive index difference between the semiconductor and air leads to total internal reflection for all but very low angles.

Another factor affecting the light output is the design of the top electrode, which must spread the current, but at the same time not block the light.

The purpose of this thesis is to investigate different LED designs regarding output, and is composed of three parts. First, a theory part, with an overview of LED physics and various ways of enhancing the light extraction, with a focus on the resonant cavity LED (RCLED). Following, a simulation section, where different kinds of conventional LEDs and RCLEDs are simulated and compared. Lastly, a section characterizing conventional LEDs and comparing different top electrodes.

This work was done at Acreo Swedish ICT AB in Kista, during the period May-December 2013.

Chapter 2

Theory

2.1 LED basics

This and the next two sections (2.1, 2.2 and 2.3) are mostly based on [1].

2.1.1 Recombination in the pn-junction

The LED is basically a pn-junction. Under forward bias minority carriers are injected across the depletion area, recombining with a majority carrier, sending out a photon with an energy equal to the band gap E_g.

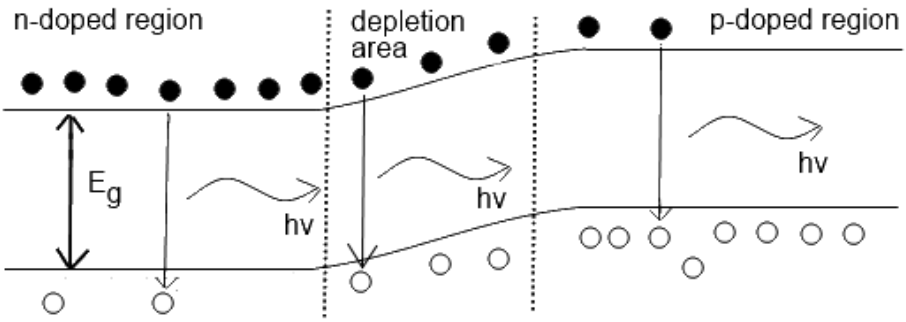

Figure 2.1: pn-junction under forward voltage.

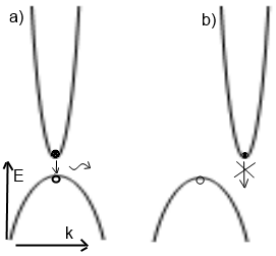

Figure 2.2: Direct and indirect bandgap. Energy E on the y-axis, wavenumber k on the x-axis.

Electrons and holes can recombine both radiatively, i.e. sending out a photon, and non-radiatively, instead sending out phonons. The momentum of a photon is very small compared to the electron momentum, practically negligible. Since the momentum needs to be conserved, the momentum at the top of the conduction band and at the bottom of the valence band needs to be the same for radiative recombination to be probable. This is called a direct band gap, in contrast with a indirect band gap where this is not the case (Figure 2.2). In the case of an indirect band

gap, almost all recombination is non-radiative. There is a possibility of radiative recombination by release of both a photon and a phonon, but since this is a three particle interaction, the probability is much lower. Both the type of band gap (direct/indirect) and it's magnitude E_g depends on the material used. Using compound semiconductor materials, ternary or quaternary III-V materials in particular, E_g can be varied, and thus LEDs of different colours can be manufactured. The probability of non-radiative recombination also increases with increasing defect concentration, by the Shockley-Read-Hall mechanism. Most LEDs are manufactured as a stack of epixatially grown layers, and modern epitaxial growth methods gives very low defect concentrations [2].

2.1.2 Heterostructures

The rate R of radiative recombination is given by the bimolecular equation

$$R = Bnp \tag{2.1}$$

Where n is the electron concentration, p the hole concentration, and B a proportionality constant. In the bulk LED pictured in 2.1, charge carriers will move on average one diffusion length from the edge of the depletion area before recombining. The minority charge carriers will thus be distributed over a quite large region, with the concentration falling the further away you get from the depletion area edge. If both charge carriers can be confined to the same place in space, increasing the concentrations, the recombination rate can be improved. Using materials with different band gaps in the same structure (this is called a heterostructure), such confinement can be realized. A low band gap material sandwiched between two layers of a higher band gap material is called a double heterostructure.

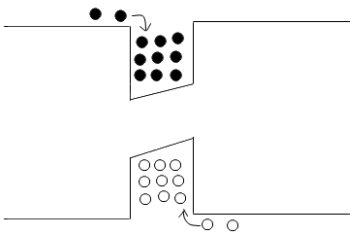

(a) Double heterostructure under forward bias.

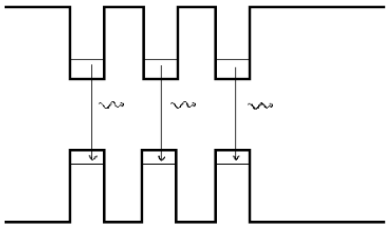

(b) MQW structure unbiased.

If this layer is small enough that quantum effects can not be neglected, it is called a quantum well (QW). A structure with many quantum wells is called a multiple quantum well (MQW) structure. In a quantum well, the lowest possible energy for a charge carrier will not be at the bottom of the band, but somewhat over that, per elementary quantum mechanics. The energy of emitted photons from a QW structure will thus be somewhat larger than E_g. This energy difference increases with decreasing well thickness, and vice versa. At high injection currents, charge carriers may be injected quicker than they can recombine. These carriers will then just travel through the device without contributing to the light output. This is called carrier overflow.

Other layers might be added to the stack in order to improve the LED. One example is the current-spreading layer. The electrode on the light emitting side (the top) can not cover the entire side, since the most metals are non-transparent. See figure 2.4. Since most LEDs have a bottom electrode that covers the entire backside, the current will spread outwards towards the sides while flowing through the stack. If the active layer is close to the top electrode, the spreading will be small, and most current will flow below the top electrode, and most of the light produced will thus be blocked. A current-spreading layer is simply a transparent, low resistivity layer added below the the top electrode so that the charge carriers will travel longer and be more spread.

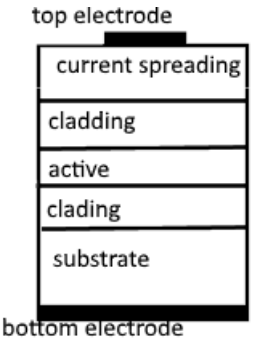

Figure 2.4: Schematic sketch of a typical LED.

2.1.3 Temperature effects

When current flows through a LED, it will heat up. This will affect the spectral properties. Firstly, the higher temperature means larger lattice vibrations, increasing the mean distance between the lattice atoms. Since the band structure is a consequence of the crystal structure, this will affect the band gap, lowering it and thus increasing the photon wavelength λ. Secondly, the spectral width is increased. The Boltzmann distribution gives a higher probability of an electron having a higher energy (or a hole having a lower energy) when the temperature is increased, meaning a larger amount of photons with a greater energy. The temperature dependence of the FWHM (see section 2.3) is

$$\Delta\lambda = \frac{18\mathrm{k}T\lambda^2}{\mathrm{hc}} \tag{2.2}$$

This spreading of the charge carriers over the states also means that the probability of the charge carriers having the same momentum decreases, leading to a lower recombination probability. A higher temperature also means a larger probability for charge carriers in heterostructures thermally escaping confinement. Thus the rate of radiative recombination is lowered by an increase in temperature.

2.2 The physics of light extraction

The main factor limiting the extraction efficiency of LEDs is the total internal reflection. The refractive index of semiconductor materials is quite high, about 3-3.5, which will lead to a small total reflection angle per Snell's law

$$n_\mathrm{s}\sin(\phi_\mathrm{s}) = n_\mathrm{air}\sin(\phi_\mathrm{air}) \tag{2.3}$$

where n_x is the refractive index of the material x, and ϕ_x is the angle of the ray in that material and s is short for semiconductor. ϕ_air can not be greater than 90°. Thus there will only exist an external ray for internal rays with ϕ_s for which ϕ_air is 90 ° or lesser. The ϕ_s for which $\phi_\mathrm{air} = 90°$ is called the critical

angle and rays with an angle greater than this will instead undergo total internal reflection. The critical incidence angle for total internal reflection is

$$\phi_{\mathrm{c}} = \arcsin\left(\frac{n_{\mathrm{air}}}{n_{\mathrm{s}}}\right) \tag{2.4}$$

Which for a semiconductor/air-interface will be 15-20 degrees. Only light that falls into this cone will escape the semiconductor material into the air. Light outside the cone will be trapped, reflected back and forth until it is re-absorbed. Assuming an isotropic emission, the extraction efficiency η_{ee} can be calculated

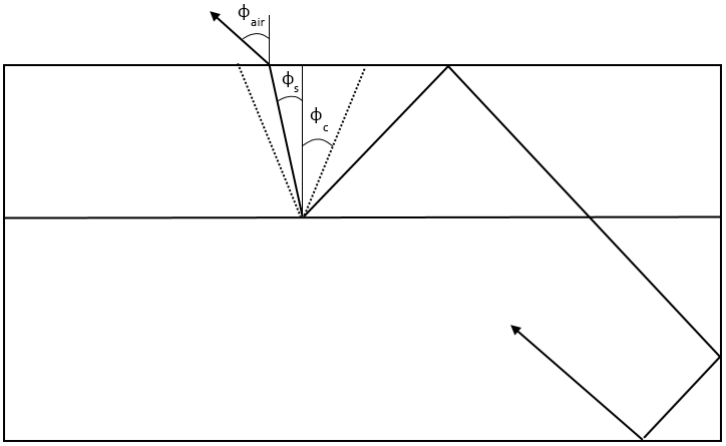

Figure 2.5: The extraction cone (dotted lines), and extracted ray (left ray) and a totally internally reflected ray (right ray) from a point source

by dividing the area that falls into the cone by the total spherical surface area. The result is [1]

$$\eta_{\mathrm{ee}} = \frac{1}{2}(1 - \cos(\phi_{\mathrm{c}})) \tag{2.5}$$

Using the critical angle calculated earlier, this will be 1-3 % for most semiconductors.

Light that does fall into the extraction cone will also be partially reflected, this is called Fresnel reflections. The reflectance, the part of the power that is reflected, can be calculated using Fresnel's equations [3].

$$R_{\perp} = \frac{n_s \cos(\phi_s) - n_{air} \cos(\phi_{air})}{n_s \cos(\phi_s) + n_{air} \cos(\phi_{air})} \tag{2.6}$$

for s-polarized light and

$$R_{\parallel} = \frac{n_{air} \cos(\phi_s) - n_s \cos(\phi_{air})}{n_{air} \cos(\phi_s) + n_s \cos(\phi_{air})} \tag{2.7}$$

for p-polarized light for light traveling trough a semiconductor/air interface. Unpolarized light contains an equal amount of both polarizations, and R is then the arithmetic mean of equations 2.6 and 2.7. This set of equations can be derived from continuity conditions on the electric and magnetic fields when crossing a material boundary. The reflectance for a semiconductor-air interface will be about 30 % along the optical axis. That means that almost at third of the small part of the light that falls into the escape cone is reflected.

2.3 Figures of merit

When comparing LEDs there are a couple of quantities that are useful. The possibility of non-radiative recombination means that not all electrons injected will produce a photon. The internal quantum efficiency is defined as the number of photons produced divided by the number of electrons injected.

$$\eta_{\text{int}} = \frac{n_{\text{int}}}{n_{\text{e}}} = \frac{P_{\text{int}}/(\text{h}\nu)}{I/\text{e}} \tag{2.8}$$

where I is the current, n_{e} is the number of electrons, n_{int} is the number of photons produced per second internally and P_{int} their power. Not every photon produced will escape the LED (see section 2.2). The extraction efficiency is defined as the fraction of photons produced that escape into the air.

$$\eta_{\text{ee}} = \frac{n_{\text{ext}}}{n_{\text{int}}} = \frac{P/(\text{h}\nu)}{P_{\text{int}}/(\text{h}\nu)} \tag{2.9}$$

where n_{ext} is the number of photons escaping from the LED, and P their power. The external quantum efficiency is defined as the number of escaped photons divided by the number of injected electrons

$$\eta_{\text{ext}} = \frac{n_{\text{ext}}}{n_{\text{e}}} = \frac{P/(\text{h}\nu)}{I/(\text{e})} = \eta_{\text{ee}}\eta_{\text{int}} \tag{2.10}$$

The power efficiency, or the wallplug efficiency, is the power of the output light divided by the input electrical power.

$$\eta_{\text{p}} = \frac{P}{IV} \tag{2.11}$$

where V is the voltage. For some applications, for example communications, a narrow spectral line width is important. This is most commonly measured using the Full Width at Half Maximum (FWHM), i.e, measuring the width of the spectrum at half the maximum intensity. See figure 2.6.

2.4 Some light extraction methods

The isotropic emission means half the radiation will be emitted downwards, towards the substrate, which in many cases will absorb that light. In this case, or if one for some other reason wants top extraction only, it is a good idea to have some kind of mirror between the component and the substrate. A distributed Bragg (DBR) reflector is easily incorporated and consists of alternating layers of high refractive index and low refractive index dielectric materials. The thicknesses are chosen so that the optical path in each layer equals $\lambda/4$. Waves reflected from each interface will then constructively interfere. The reflectivity R along the optical axis of a quarter-λ layer stack is as follows [4]:

$$R = \left[\frac{n_s n_2^{2m} - n_e n_1^{2m}}{n_s n_2^{2m} + n_e n_1^{2m}}\right]^2 \tag{2.12}$$

where s refers to the medium where the light originated, 1 and 2 to the layer materials, and e to the exit material.

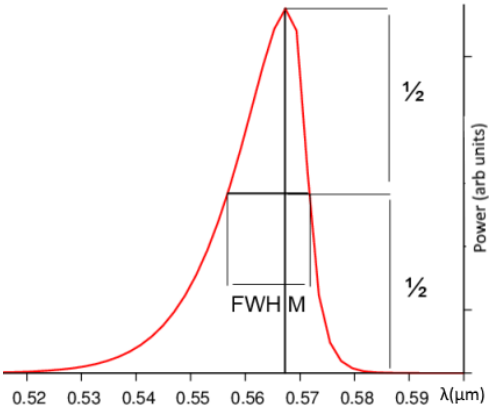

Figure 2.6: The definition of the Full Width at Half Maximum (FWHM). This example is a simulated LED spectrum

Another method for enhancing the η_{ee} is to put an antireflective layer on top. This is the opposite of a DBR, where instead the layer thickness and refractive indices are chosen so that the forward going waves interfere constructively. This will eliminate or at least decrease the Fresnel reflections. For a single layer the optical path length should be $\lambda/4$, the reflectance for normal incidence is then

$$R = \frac{\left(n_e n_s - n_1^2\right)^2}{\left(n_e n_s + n_1^2\right)^2} \tag{2.13}$$

so $R = 0$ if $n_1 = \sqrt{n_e n_s}$ [5]. If there is no usable material with that refractive index, a multilayer stack can be designed.

Since the problem of total internal reflection is caused by a too steep angle between the ray of light and the surface, shaping the surface can reduce the angle, leading to extraction immediately or after a few reflections. The optimal shape would be spherical, but that is hard to combine with standard planar semiconductor technology. LED chips in the shape of a truncated inverted pyramid with an η_{ext} of 55 % after packaging has been manufactured by sawing, a method suitable for mass production [6, 7].

The idea behind surface texturing, sometimes called surface roughening, is the same as for chip shaping, but at a smaller scale. Light impinging on a textured surface and not immediately extracted might be after a few reflections, since the angle will not be the same every time it hits the surface. A textured surface can be made by intentionally growing a rough film on top[8], or by etching [9], or by depositing nanosized particles on top [10]. An η_{ext} of 54% after encapsulation has been observed for a surface textured LED with a back reflector [11].

The standard encapsulation of the LED chip in a dome-shaped polymer capsule with an n_{e} higher than air will increase the η_{ee}. The critical angle at the semiconductor-encapsulant interface will be larger than that at the semiconductor-air interface, extracting more light. The dome shape of the capsule means that all rays in the encapsulant, regardless of direction, will make a normal angle to the encapsulant-air interface, and thus all be extracted. The

ratio of the η_{ee} for the encapsulated and the unecapsulated case can be written

$$\frac{\eta_{\text{enc}}}{\eta_{\text{unc}}} = \frac{1 - \cos(\phi_{\text{c,enc}})}{1 - \cos(\phi_{\text{c,air}})} \tag{2.14}$$

where $\phi_{\text{c,enc}}$ is the critical angle for the semiconductor-encapsulant interface, and $\phi_{\text{c,air}}$ the critical angle for the semiconductor-air interface. A typical LED will improve its η_{ee} by a factor 2-3 upon encapsulation in a material with a refractive index of 1.5, and more if the the refractive index is larger [1].

2.5 The resonant cavity light emitting diode

Proposed by Schubert [12], the idea behind the resonant cavity LED is to use the constructive and destructive interference to redistribute the emission over the angles, so that a larger part of the emission falls into the light extraction cone. This is done by putting mirrors on top and at the bottom of the LED stack. The reflected waves will then interfere with each other, some constructively, some destructively, depending on the angle. The waves that interfere constructively will be enhanced, and are called resonant states and the ones that do not will be suppressed and are called non-resonant. The criterion for constructive interference is that the phase difference is a integer number of periods, i.e that the waves are in phase. For two waves that have traveled different paths to fulfill this, the optical path difference must be an integer number of wavelengths. Under the assumption of no phase shift upon reflection, this means that for the on-axis wave, to be resonant the optical path length of the cavity needs to be an integer number of half-wavelengths. At other angles, the waves see the longer cavity $dn\cos\theta$, where d is the geometrical length of the LED and θ is the emission angle. The general criterion for resonance is thus

$$d * n\cos\theta = m\lambda/2 \tag{2.15}$$

where λ is the wavelength and m is any integer. Introducing the cavity order $m_{\text{c}} = dn2/\lambda$, the criterion can be rewritten as

$$m_c\cos\theta = m \tag{2.16}$$

Thus, the number of resonances can not be greater than m_c. In a $\lambda/2$-cavity, the only resonance will be the on-axis one, and all emission will fall into the extraction cone. Longer cavities will have more resonances, spread over θ, meaning that less of the power will be extracted. A rough approximation of the extraction efficiency can be calculated by dividing the number of resonances in the extraction cone by the total number of resonances m_c. Real mirrors have a non-zero phase shift. The penetration depth is the distance you would have to shift an ideal mirror (a mirror with no phase shift) to give the same phase shift. This means that the effective cavity length and effective m_c is somewhat larger than above.

To be able to extract light, one mirror needs to have a reflectance lower than 1. For the other, the reflectance should be as close to 1 as possible, forcing the extraction through only one facet. The higher the reflectance of the output mirror, the more round trips the average photon makes in the cavity before extraction. This means a higher probability of re-absorption. Higher reflectivites

also means a smaller width for the resonance peaks, meaning a lower FWHM for the extracted light, but also that the light on the lower and higher edges of the internal emission peak will not be extracted, lowering the total power output. In total this means a moderate reflection of the output mirror gives the best results.

Even though the best RCLEDs have a short cavity, output enhancement has also been observed for long cavities [13].

Chapter 3

Simulation

The following simulations were run to investigate if the light extraction of a long LED structure could be improved by making it a RCLED and to investigate how different structures affected parameters such as output power and spectral width . The simulations were done in the semiconductor simulation software APSYS [14]. One green-emitting bulk structure and one red-emitting MQW structure were simulated both as ordinary LEDs and RCLEDs. For the ordinary LEDs the LED module was used, and also the ray-tracing module for calculating the extraction efficiency. For the RCLEDs the RCLED module was used. For the quantum well structure, the quantum transport and, for some runs, the self-consistency modules were used.

3.1 The green LED

The green structure simulated can be seen in figure 3.1. The upper and lower surfaces are used as contacts in the simulation. The peak wavelength is at

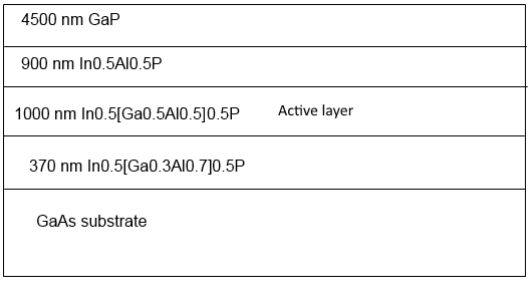

Figure 3.1: Green simulated structure. Not to scale.

about 568 nm. The different curves in 3.2 are the spectra for different currents, where a higher current gives a higher peak. The FWHM is about 14-15 nm. The raytracing module calculates the extraction efficiency to be about 1 %. Using the refractive index 3.41276 [15] for GaP in formulas (2.4-2.5) gives a extraction of about 2.2%. Simulations at different temperatures were run to test the temperature dependence of the optical properties.

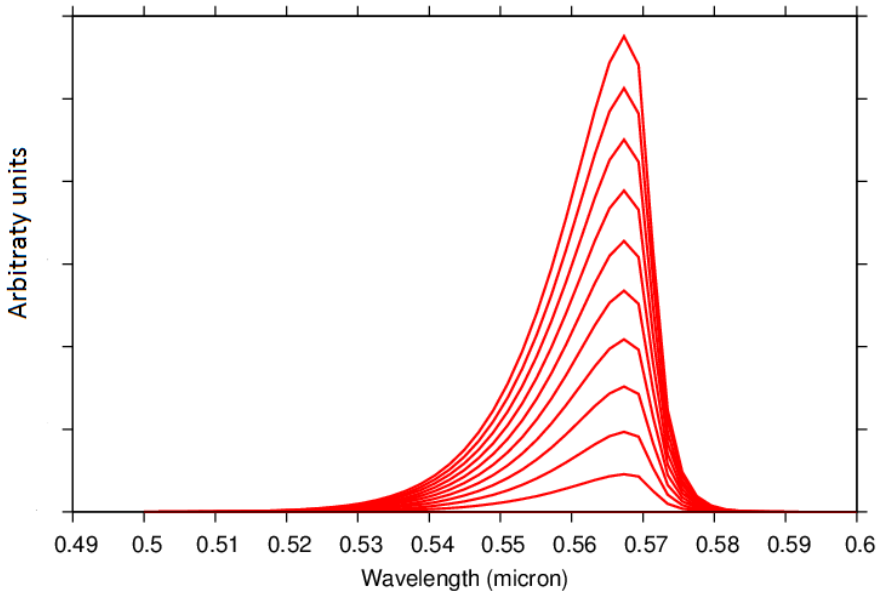

Figure 3.2: Green LED spectrum.

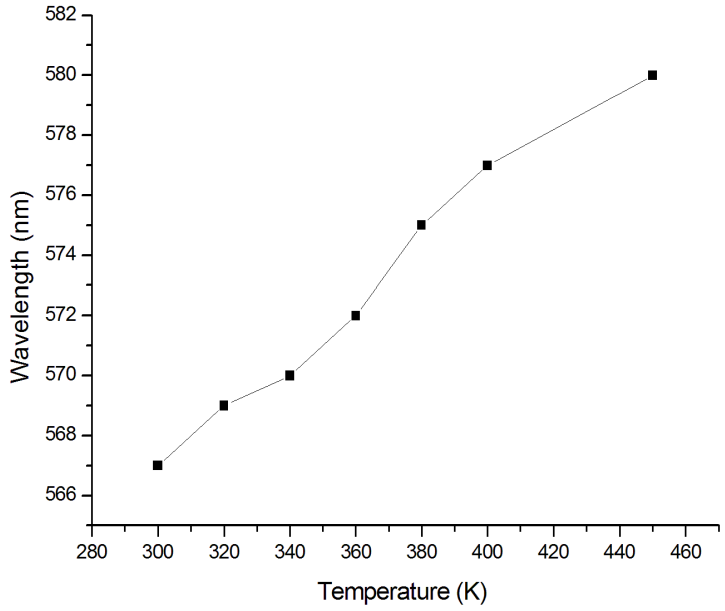

Figure 3.3: Peak wavelength temperature dependence

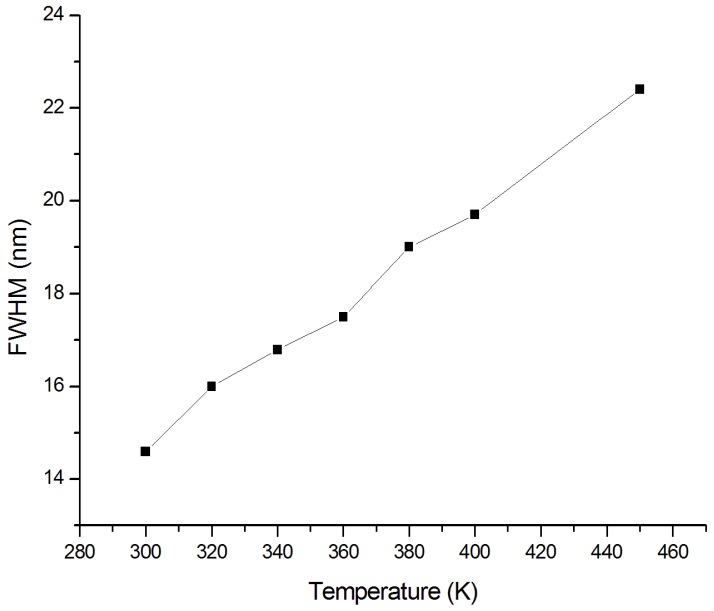

Figure 3.4: FWHM temperature dependence.

In Fig 3.3 and Fig 3.4 shows that both the peak wavelength and the FWHM increase with temperature, in accordance with the theory.

3.2 The green RCLED

The structure simulated is the same as earlier, but with the substrate removed and replaced with a metal mirror with R= 95% at that end and a DBR-structure with a varying number of layer-pairs at the other. The DBR is made of alternating layers of SiN and SiO. These two mirrors enclose and define the resonant cavity. Light is extracted from the DBR side. Simulations are run with 1-5 layer pairs with SiN closest to the component, and 2-3 layer pairs with SiO closest to the component.

The results are summarized in table 3.1. The reflectances are in the direction normal to the plane.

Looking at the table we see that the two and three pair structures has reflectances of 1-2 % and are thus not DBRs at all, but rather anti-reflection layers. Thus, the high extraction efficiency calculated for those structures is probably not the true value, the ability of the RCLED module of the program to accurately simulate a non-resonant structure being uncertain. For the rest of the structures, the DBRs are actually reflecting, and we can see the resonance peaks in the spectrum (see figs 3.5 - 3.6). Because of the long cavity, there are quite a few peaks in the spectrum, all inside the envelope function of the unresonant spectrum. The FWHM of the peaks decreases with increasing reflectance. The

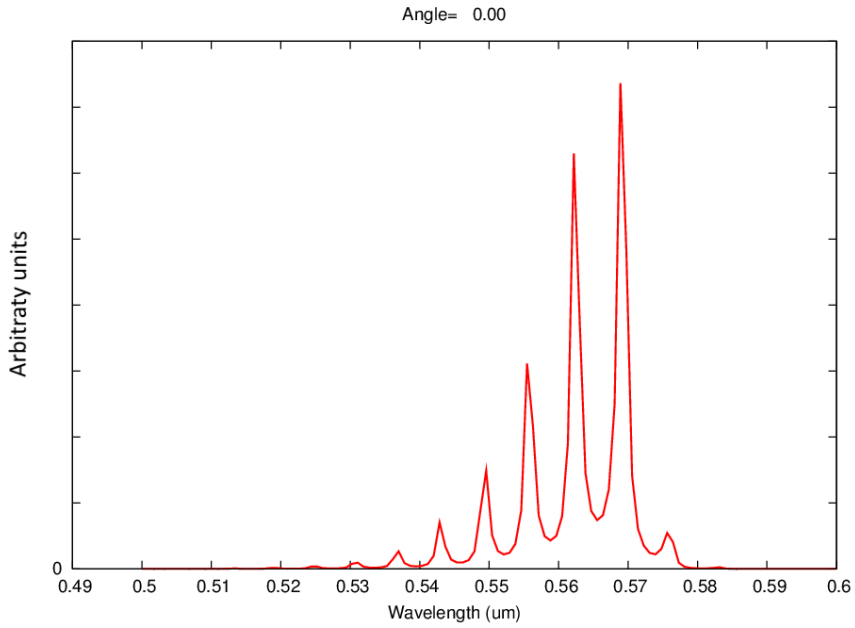

Figure 3.5: Spectrum for 6 DBR-pairs at zero angle

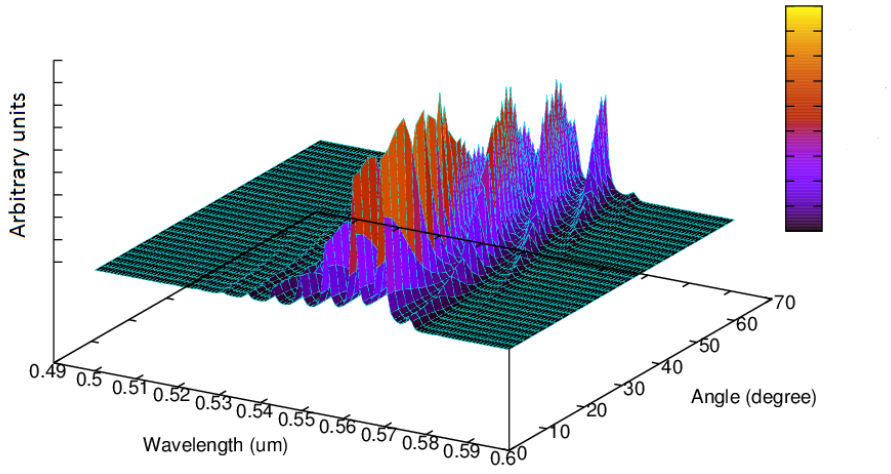

Figure 3.6: Spectrum for 6 DBR-pairs as a function of wavelength and angle

Pairs	R(%)	η_{ee} (%)	P (mW)	FWHM highest subpeak (nm)
Ordinary LED for comparison				
0	–	1	0.3	15
SiN/SiO				
1	11	14	5.7	5.6
2	1	24	9.3	15
3	2	20	8	13
4	15	13	5.4	3.7
5	33	8	3.2	2.7
6	52	5	2	2
SiO/SiN				
2	65	1.6	0.7	1.3
3	77	0.7	0.3	1.3

Table 3.1: Results of RCLED simulation.

resonant cavities does have an increased extraction efficiency compared to the conventional LED, but the extraction does fall with increasing R, with the R=77% structure being worse than the conventional LED. The active layer is quite thick, so the probability of reabsorbtion is quite high, pushing the optimal R down. A greater control over R can be had if one uses a material pair with a smaller refractive index difference. Then R will not increase as much per layer pair, as per equation 2.12. This is not done in this thesis. Fig 3.6 shows the spectrum at different angles. We see that the peak wavelengths shift as the angle and thus the optical path length increases. The internal production also increases by 33 %, compared to the ordinary LED.

Another set of runs, with the placement of the mirrors switched were also run. The results are the same, the extraction efficiency and the FWHM just

Pairs	R(%)	η_{ee} (%)	P (mW)	FWHM highest subpeak
SiN/SiO				
1	11	13	5.3	3.6
2	1	22	8.5	15.8
3	2	17	7.1	6
4	15	10	4.2	3.3
5	33	3.5	1.68	1.6
6	52	2	1	1.3

Table 3.2: Results of RCLED simulation with the metal mirror on top and the DBR at the bottom.

dropping slightly.

DBRs with TiO/AlO instead of SiN/SiO where also run. Because of the higher difference in the refractive indicies, the reflectance at the same number of pairs is higher than for the SiN/SiO-DBRs. The extraction is thus somewhat lower at the same number of pairs.

The previous simulations were just adding the resonant cavity structures to a given LED-structure, without caring if the cavity was an integer number of wavelengths. Since the cavity is long, and the light is not monochromatic,

Pairs	R(%)	η_{ee} (%)	P (mW)	FWHM highest subpeak
TiO/AlO				
1	5	16	6.7	9.4
2	3	21	8.5	11
3	26	10	4.3	2.3
4	55	2.5	1.1	1

Table 3.3: Results of RCLED simulation with metal oxide DBR.

the probability of no part having a resonance is very low. But how will the extraction be affected if we center the resonance on the peak wavelength? The thickness of the GaP layer in the 5 pair SiN/SiO DBR at the bottom structure was varied until the highest peak was centered at the peak wavelength of 569 nm, giving a thickness of 4.375 μm. The extraction efficiency increased from 3.5 % to 6 %, and the output power from 1.68 mW to 3mW. Reducing the GaP layer further to 0.5 μm reduces the number of peaks to three, as can be seen in figure 3.7, and increases the extraction efficiency to 6.8 % and the power to 2.9 mW). This cavity is again not an integer number of half-wavelengths. Because of the way the bias is applied in the simulation, where the whole top and bottom areas are used as electrodes, any decrease in current spreading and any following decrease in output caused by the shorter current-spreading layer is not taken into account in this number.

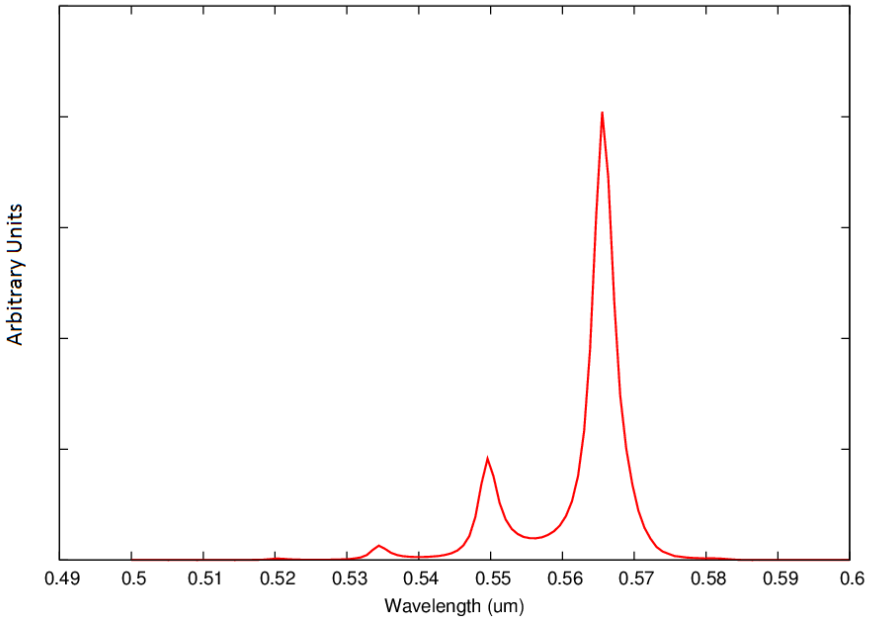

Figure 3.7: Spectrum of Green RCLED with 0.5 μm GaP-layer.

3.3 The red LED

The simulated red structure can be seen in figure 3.8 below. This is a multiple quantum well (MQW) structure, with a well and barrier width of 10 nm.

GaP	1600 nm
In0.5Al0.5P	400 nm
In0.5(Ga0.3Al0.7)0.5P	200 nm
MQW 10*In0.52Ga0.48P wells 10 nm In0.5(Ga0.5Al0.5)0.5P barriers 10 nm	
In0.5(Ga0.5Al0.5)0.5P	2000 nm
In0.2Ga0.8As0.5P0.5	50 nm
In0.5Ga0.5As0.2P0.8	100 nm
GaAs substrate	

Figure 3.8: Simulated red structure. Not to scale

In figure 3.9 we see the band structure of the quantum wells, with the calculated quantum states printed.

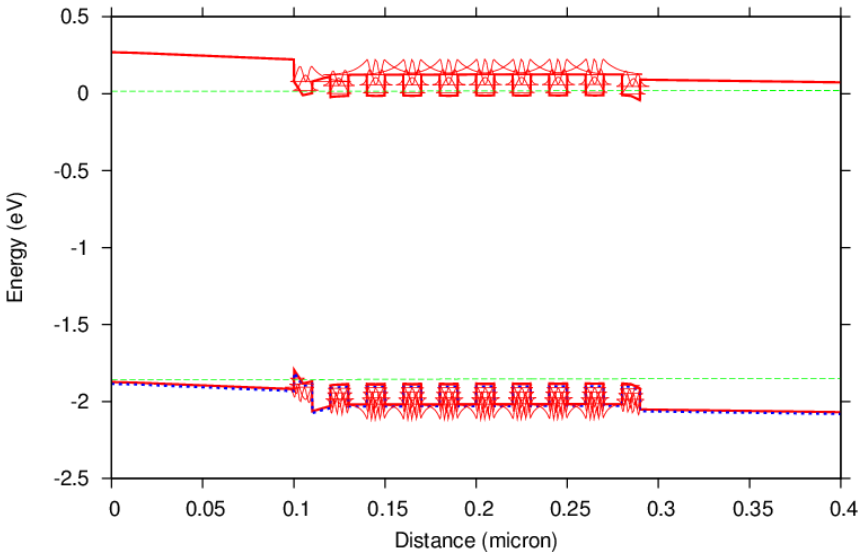

Figure 3.9: Band structure and quantum states of the red MQW.

If we vary the quantum well thickness the emitted wavelength changes, as can be seen in figure 3.10. We see that the wavelength stops changing at a quite low width of about 8 nm. The electrons stops being confined and start acting as bulk electrons. The structures with a smaller well width has a lower η_{int} than the wider wells, probably because of carrier overflow.

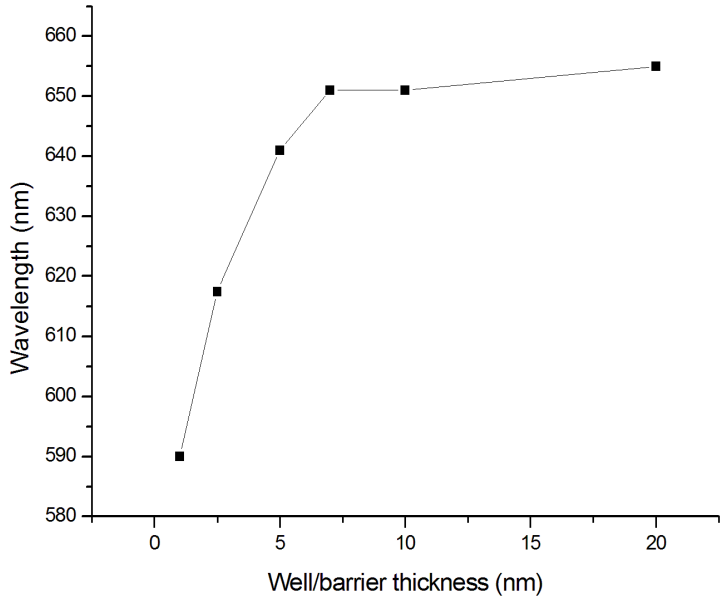

Figure 3.10: Wavelength dependence on well width.

The raytracing module gives an extraction efficiency of 3.4 %. This is quite a bit higher than the green LED. Using the same procedure as for the green LED it should be 2.3 %.

3.4 The red RCLED

The simulation is performed for a red LED with the same metal back mirror and SiN/SiO DBR as for the green RCLED, but with the DBR layer widths adjusted to match the new wavelength. The results turned out to be very similar to the green RCLED.

The results are collected in table 3.4. We see that the RCLED does enhance the extraction somewhat at lower reflectivites, but since the plain red LED had a higher extraction efficiency to start with, the enhancement is not as great as for the green RCLED.

3.12 shows the emission pattern for the RCLED design with a four pair DBR. We see that the maximum power is not at a 0° angle but at 22°. This is caused by some cavity at an angle to the optical axis being more optimal than the on-axis cavity. That this might happen is not surprising, given that the on-axis cavity length is not optimized in these simulations. This effect might not be wanted for certain applications.

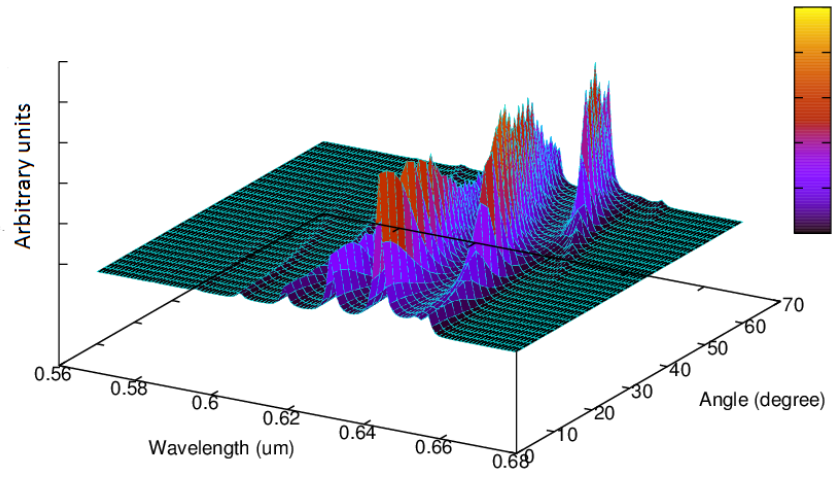

Figure 3.11: Red RCLED spectrum for 5 pair DBR.

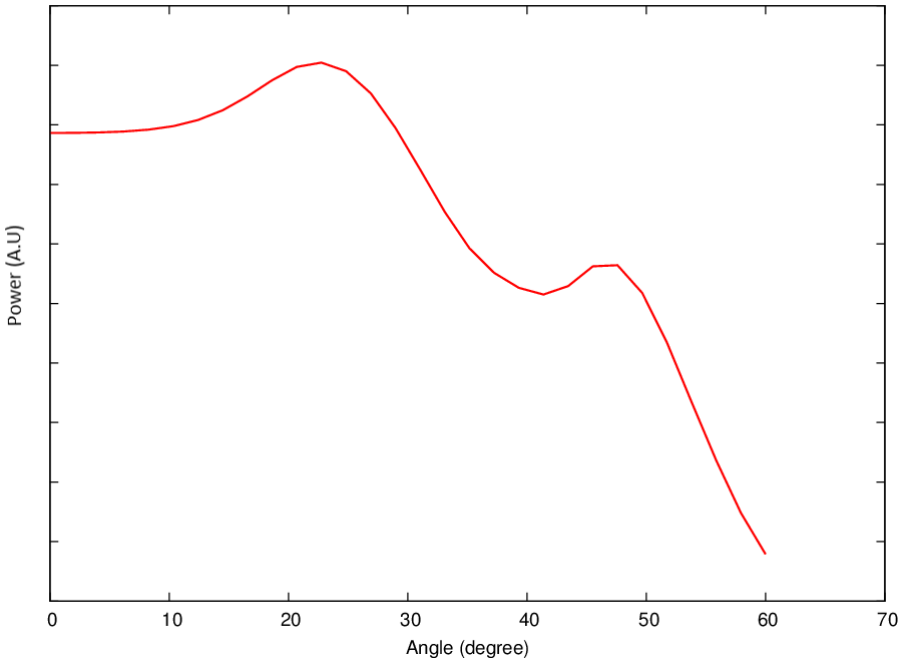

Figure 3.12: Emission pattern for a red RCLED with a four pair DBR

Pairs	R(%)	η_{ee} (%)	P (mW)	FWHM highest subpeak
Ordinary Red LED for comparison				
0	–	3.5	1.3	22.5
SiN/SiO				
1	10	9	2.8	5.2
2	0.5	16	6.1	18.6
3	3	12	4.6	13.1
4	17	6	2.3	4.1
5	37	3.7	1.8	2.5

Table 3.4: Results of red RCLED simulation.

Chapter 4

Electrode fabrication

The top electrode geometry has a direct effect on the output power. An even spreading of the current is wanted, to avoid local heating and overflow effects lowering the output power. A spread out current is accomplished by a spread out electrode. Since metal is not transparent, the electrode will block light produced underneath it, so the area covered by the metal should be small. Based on this, a grid or web shaped electrode seems like a good idea [16, 17]. Three of the four electrode geometries used can be seen in figure 4.1.

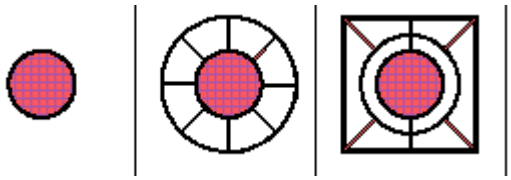

Figure 4.1: The different electrode geometries. From left to right: Type A,B,C. Type D not shown, but it is also of a spread shape. The checkered areas are the bond pads.

Electrodes were manufactured on four wafers, two with a green emitting LED structure and two with a red emitting structure, using a mask with the different geometries in figure 4.1 in different sizes. These are conventional LEDs, i.e not RCLEDs. To be able to wire bond the components upon packaging a bond pad, a part with thicker metal, is needed. On two of the wafers a silicon nitride (SiN) layer is deposited underneath the bond pads, the idea being that this should work as a current blocking layer, forcing the current out from the volume underneath the bond pad, hopefully instead flowing through, and producing light in parts of the component that are not shadowed, increasing the output power. See figure 4.2

The needed process steps thus are

1. SiN deposition (two wafers)
2. top electrode deposition
3. bond pad plating
4. thinning

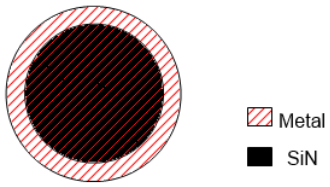

Figure 4.2: The silicon nitride layer underneath a type A electrode seen from above.

5. bottom electrode deposition

After cleaning of the wafers, a SiN layer is deposited on half the wafers by Chemical Vapour Deposition (CVD). In all types of CVD, precursor gases are pumped into the reaction chamber where they are adsorbed onto the wafer surface. Here they react with one another, forming the desired film. Any gas phase byproducts are pumped away. This process covers the entire surface with SiN. To define the current blocking layers, parts of the SiN layer must thus be removed and this is done by etching. The areas to be etched are defined by a photolithography process. The wafers are put into a spinner, and resist is deposited onto the surface, the spinning motion spreading it into an even layer. A resist is a polymer solution, that upon exposure to UV radiation changes it's properties, becoming easier or harder to dissolve in a solvent, called a developer. To only expose the areas of the resist that are to be altered, it is exposed to UV light through a mask, that blocks the light from reaching the areas that are not to be exposed. The resist is then developed, removing the altered areas. The SiN is then etched by reactive ion etching, followed by stripping (removal) of the remag resist. After this, the processing is the same for all four wafers.

A second photolitography process, for the electrodes, follows.Two layers of resist are consecutively spun on, this for easier lift off, lift off being the stripping of resist (called a lift off layer in this case) after deposition of metal over the entire surface, leaving only metal in the photolitographically opened windows. The double layer is exposed to the mask and developed. The electrode metal is evaporated onto the wafer by electron beam evaporation, i.e an electron beam is set on a metallic source, heating and evaporating the metal, which then condensates on the wafer surface. The bond pad will be electroplated on, which means a metallic seed layer will have to be deposited first, which is done by sputtering. After photolitography, the bond pads are electroplated. The resist is stripped and the metal/seed layer between the bond pads is etched away.

Finally, the wafers are thinned down to desired thickness by grinding away the back/substrate side. This is down in two steps, one coarse grind and one finer polishing step. The bottom contact is then deposited on the entire backside, again by e-beam evaporation. The wafers are then cleaved into smaller pieces, which were then used for the measurements.

Chapter 5

Device characterization

5.1 Measurement setup

Measurements were done to evaluate which electrode gives the most output power, and also to check the spectral (wavelength, FWHM) and electrical (I-V curves) properties. The measurements were carried out on smaller wafer pieces, each piece containing hundreds or thousands of components. A probe station was used to contact the components with an optical microscope mounted above the sample to collect the light. On top of the microscope a CCD-camera for imaging was mounted. The camera could be exchanged for a silicon photo diode power sensor, or an optical fibre. The photo diode was coupled to a power meter and the optical fibre to a spectrometer. Inside of the probe station is a metal chuck, on which the wafer pieces where mounted with silver glue. This chuck also served as the electrical contact to the bottom electrode, the top electrode being contacted with one of the probe arms. The I-V curves were measured with a parameter analyzer.

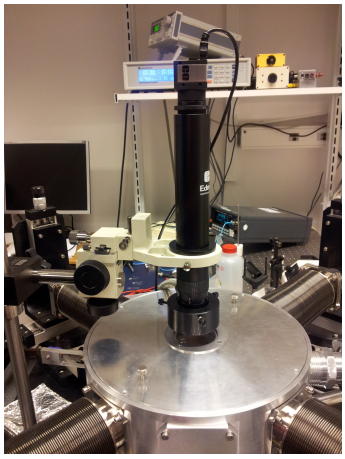

(a) Probe station.

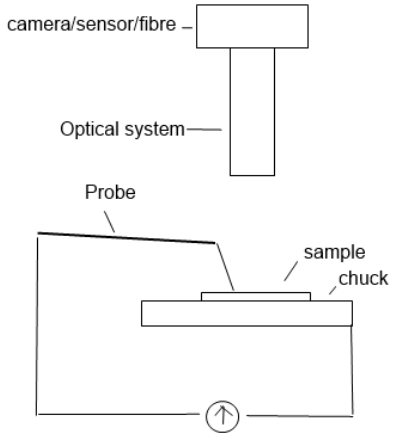

(b) Schematic picture of probe station setup.

The design of the probe station limits how close to the sample the aperture

of the optics can be, and thus how much of the emitted light can be collected. The distance is measured with a ruler to be about 7 cm, and the diameter of the lens to be 1.5 cm. Thus the half-angle of the emission cone captured by our setup is about 6 °. An unpackaged LED should have a lambertian emission pattern, i.e

$$I = I_0 \cos(\phi) \quad [1] \tag{5.1}$$

Integrating over a spherical cap gives the power emitted into cone with half-angle ϕ_c as

$$P = P_0 \sin^2(\phi_c) \tag{5.2}$$

Since $\phi_c = 6°$, we only capture about 1 % of the emitted light.

5.2 Measurements

Measurements were taken from the green-emitting wafer without SiN for all four electrodes, and also for type B from the wafer with SiN. 20 components of each type were measured. From the red-emitting wafer without SiN, test structures with different size of type A were measured. For these, only five components of each size were measured. Because of time constraints, not everything is tested. In figure 5.2 it is marked where on the wafers the components measured were taken from. Also, a chip, 200 µm by 200 µm was cut from the red wafer without SiN, with an electrode of type A, and mounted on a piece of printed circuit board (PCB), with the chip bottom glued to one of the conductive tracks and the top electrode wire bonded to another track. This enabled the chip to be contacted outside the probe station and measurements to be done on a single device. In case there is any difference depending on the position on the wafer, the most likely case is that the properties have a radial dependence, i.e that components further out on the wafer differ from those closer to the center. Type C is measured on a line from the edge along the piece inwards and no change is seen in the spectral properties. The power further out is somewhat smaller (10 % difference), but this is probably because of a patch of low quality metal in the electrodes, caused by being close to a holder during electroplating. The red test structures at the very edge do differ in both spectral properties and power. Conclusion: There is some variation in the thickness of the layers at the very edge, but not elsewhere.

5.2.1 Current-voltage characteristics

Figure 5.3 shows a LED under operation.

Figure 5.4 shows the typical current-voltage dependence for the different electrodes. We see that each curve is composed of a linear part at low voltages (especially pronounced for types A and D) and an exponential part at higher voltages. The exponential part is where the diode is conducting well and thus dominating. The linear part is a parallel parasitic resistance dominating the behaviour when the conduction through the diode is small. The curve for the pcb-mounted chip (fig 5.5) is much more ideal, both in the sense that it is closer to the ideal diode equation and in the sense that the parallel resistance is unwanted. Thus, the parallel resistances in 5.4 is probably not a property of the components or the electrodes, but some side effect of the how the measurements

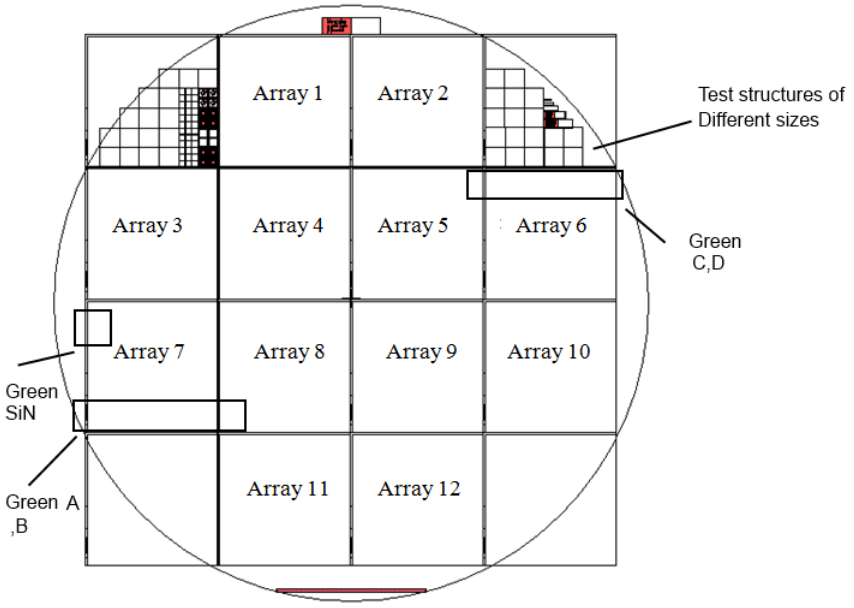

Figure 5.2: Map of a wafer.

Figure 5.3: Type C electrode at 7 mA (left) and 20 mA (right). In the 20 mA picture the camera is saturated, the light is not really white

are carried out. There might be some edge conduction of different magnitude for different sized pieces, or conduction over some defect far away from the measured component, or even some of the silver glue used for mounting the pieces creeping up the edges. Since U=RI, this parallel resistance can be evaluated as the inverse of the slope of the linear part. Doing this for one of the Type A electrodes gives a resistance of 246 Ω. In order to do a current division between the parallel resistance and the diode, the diode is approximated as a resistance with resistance equal to the inverse of the slope of a linear approximation of the exponential part of the plot. This resistance evaluates to 13 Ω, and current division gives that about 95 % of the current should go through the diode when it is the conducting state.

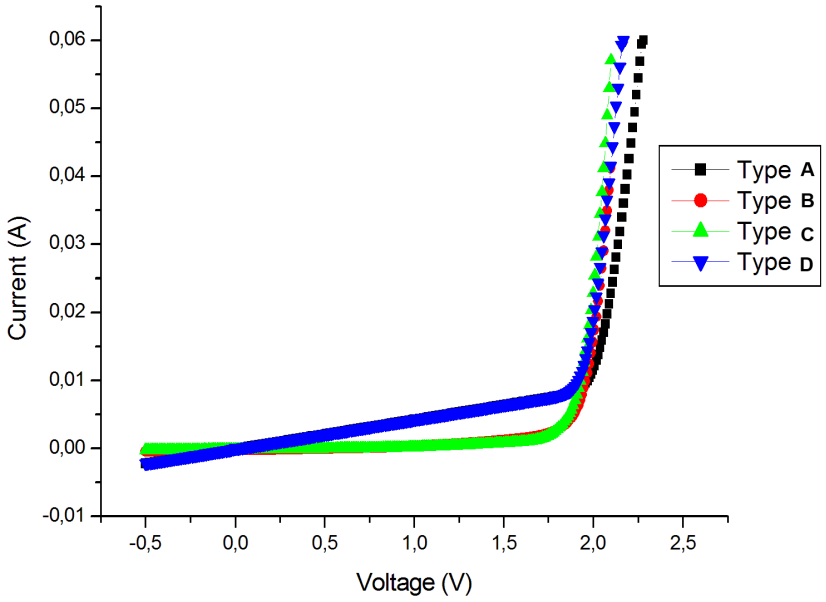

Figure 5.4: I-V curves.

5.2.2 Current-power dependence

In fig 5.6 we see that the wavelength and FWHM increases with current, as expected (compare section 2.1.3). This could not be seen in the simulations, because heating was not taken into account there (see fig 3.2. It can been seen in the simulations where the temperature was changed manually, though (fig 3.3)). The red LEDs (on wafer) behave qualitative the same as the green one in 5.6, but centered at 655 nm instead.

In 5.7 we see how the output power from a green LED first increases linearly with increasing current, falling off at 50 mA and saturating at 150 mA. This can be caused by two things, overflow and/or the higher probability for non-radiative recombination at higher temperatures. Since this is measured on a

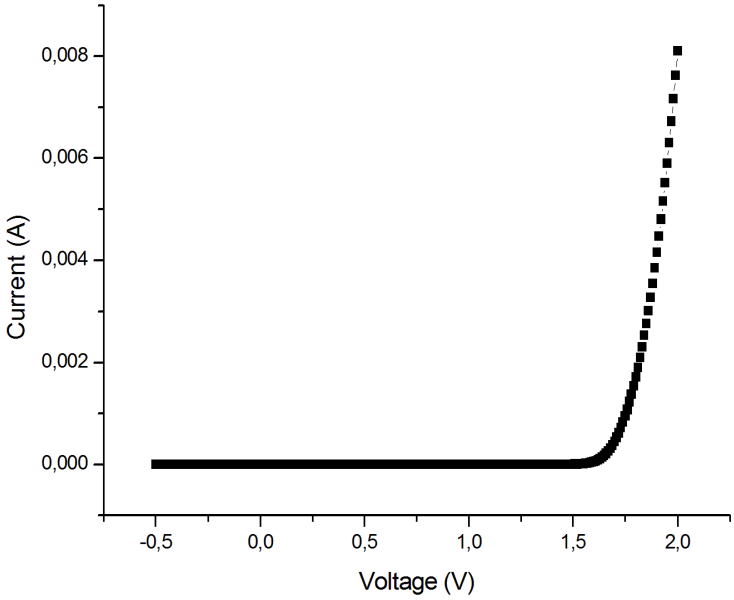

Figure 5.5: I-V for chip.

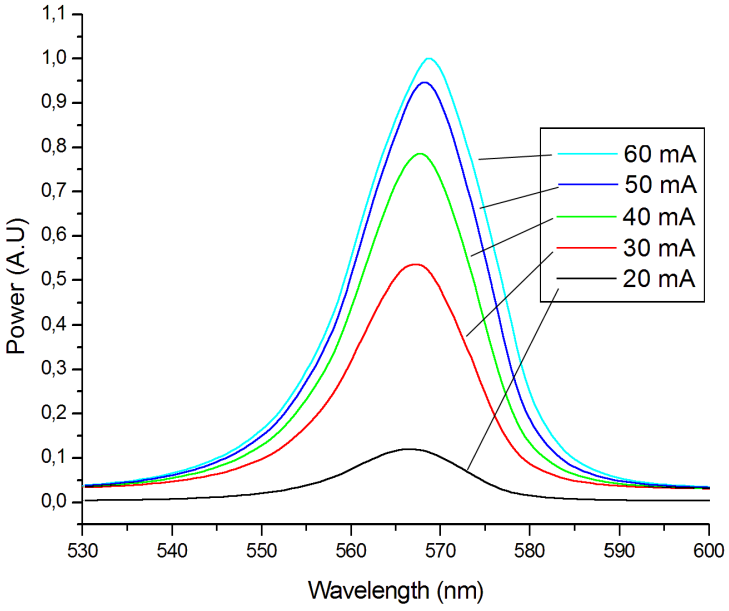

Figure 5.6: Spectra at different currents.

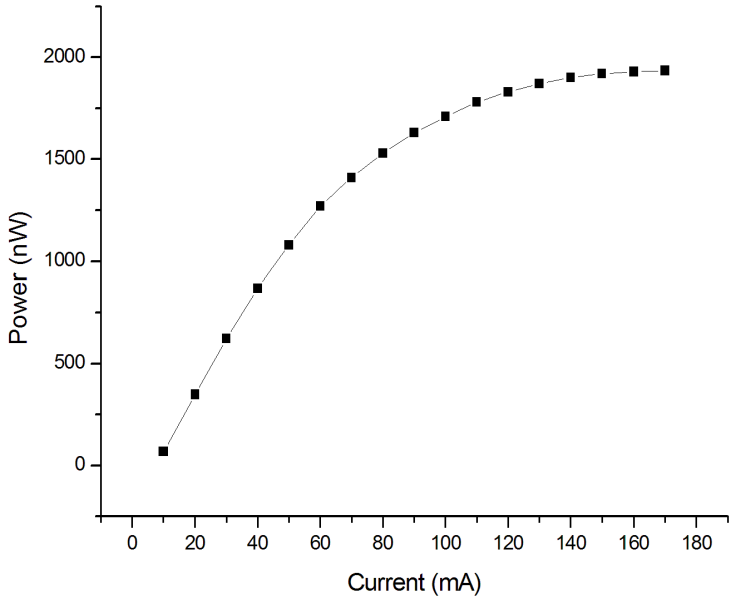

Figure 5.7: Power as a function of current Type D electrode.

piece of wafer, put on a metal chuck, the environment will cool the component more than what would be the case for a single chip, which we will see later.

When measuring the power of the chip, the power meter can be put (almost) directly on top of the chip, collecting a greater part of the emitted light. This cannot be done inside the probe station, the probes are in the way. The power 50 μW was measured at 20 mA. If we put the chip into the probe station and measure the power the same way as with the wafer pieces, we get 1.5 μW, meaning that the probe station measurements capture about 3 % of the emitted power. This is consistent with the earlier estimated value of 1 %. 1.5 μW is also bigger than the powers measured in section 5.2.4 by a factor 1.6. As seen in 5.5, there is almost no parasitic parallel resistance, which means that all current goes through the diode, increasing light output. Extraction at the sides might also increase the output. Another factor lowering the light output of the wafer measurements is that light emitted at higher internal angles will be spread out in the wafer instead of being trapped inside the chip. In the latter case, there is a chance of re-absorption and re-emission into the extraction cone, whereas in the former case any re-emission will happen somewhere outside of where the equipment is measuring.

In fig 5.8 we see that wavelength and FWHM, as a function of current, increases faster than for the component measured on wafer pieces. The peak wavelength power even decreases at really high currents. This is because of the worse thermal management for the chip, compared to the wafer pieces. The PCB has much lower heat conduction than the chuck in the probe station.

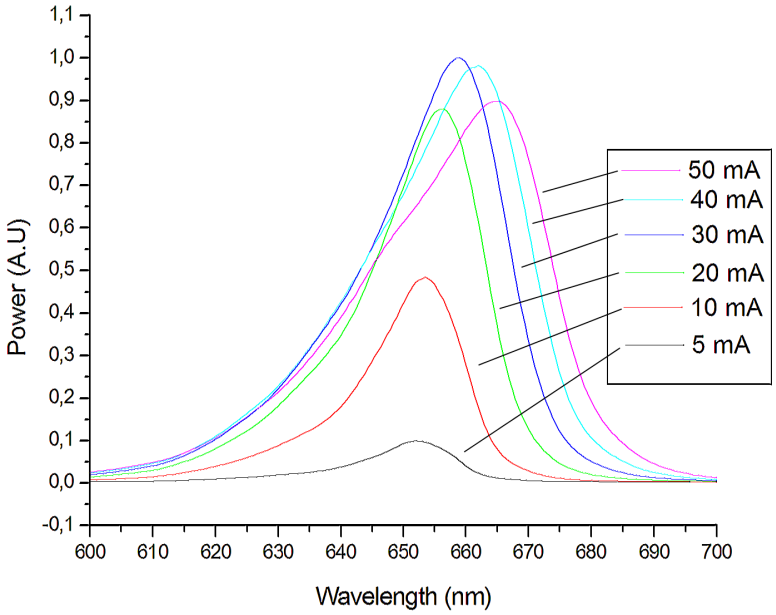

Figure 5.8: Spectra for different currents for chip.

5.2.3 Comparison between different types of electrodes

Type	P_{out} (nW)	λ_p (nm)	FWHM (nm)	V_{10} (V)
A	73	566.10	15.40	2.02
B	181	566.53	15.40	1.92
B SiN	241	565.81	15.40	1.95
C	253	566.78	15.60	1.93
D	324	566.80	15.62	1.96

Table 5.1: Comparision of different electrodes.

Table 5.1 shows a summary of the measurements on green LEDs with different electrode geometries. The power and spectral properties are all measured at 20 mA. V_{10} is the voltage required to drive a 10 mA current. We see that type D outputs the most power and that the spectral properties are unaffected by electrode geometry. We also see that the electrode with the SiN layer outputs more power than the same geometry without the SiN, without any changes in the electrical or spectral properties.

5.2.4 Comparison different size electrode

Type A electrodes of different sizes where also compared. Figure 5.9 shows a close up of figure 5.2 showing where the wafer piece with different sized electrodes was taken from. The diameter in µm of each kind is indicated in the

figure. Diameter 100 µm is the "standard" size and the size of all electrodes measured earlier in the text.

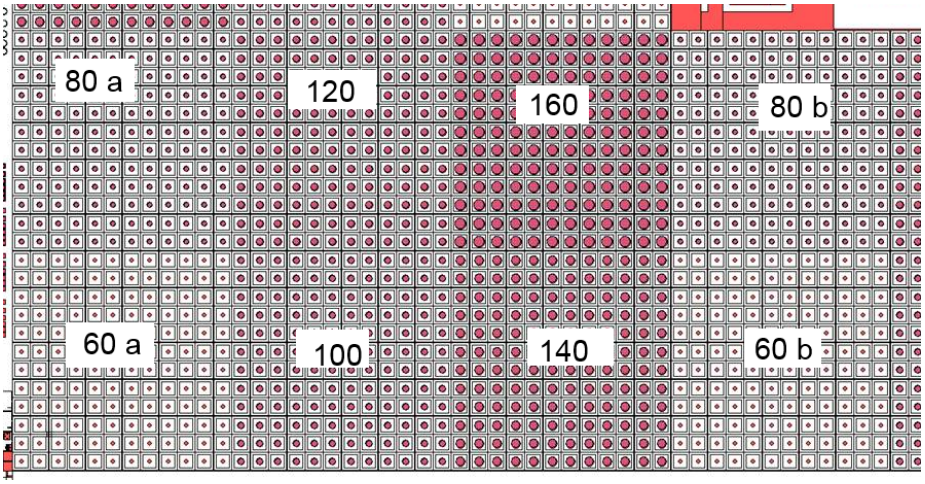

Figure 5.9: Map of test structures measured without SiN. Diameter given. Edge of the wafer to the right.

Size	P_{out} (nW)	λ_p (nm)	FWHM (nm)	V_{10} (V)
60 a	1369	652.48	19.66	>2.1
60 b	1099	654.71	20.18	>2.1
80 a	1325	652.45	19.64	>2.1
80 b	981	655.92	19.80	–
100	1172	653.02	19.05	2.05
120	1056	653.44	18.80	2.01
140	963	653.62	18.47	1.95
160	785	654.11	18.25	1.96

Table 5.2: Comparision different sizes without SiN

Table 5.2 shows the measurement results. There is a clear trend where smaller electrodes output more light. Even though electrodes of the same size farther out on the wafer output less power, fig 5.10 clearly shows a greater output for smaller electrodes. The fact that the smaller electrodes farthest out output more than the larger ones closer to the centre is evidence that the power difference is not only because of the position on the wafer. The smaller electrodes needs a somewhat larger voltage to drive the same current.

5.2.5 Reliability test

To test the reliability of the diodes, diodes of type D were left running for longer times. One run of 24 hour and one run of 72 hours. There was no change in the spectral properties, but the output power decreased to 95 % and 89 % respectively.

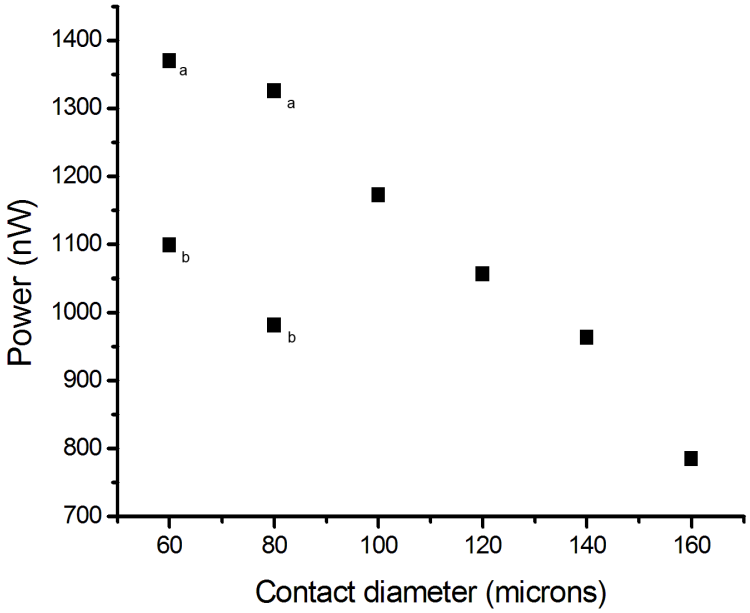

Figure 5.10: Output power for different sizes.

Chapter 6

Conclusions

6.1 Conclusions of the simulations

The simulation indicates that the emitted power of long structures can be improved by introducing a resonant cavity. This improvement is realized even if mirrors are added without taking care to set the cavity length to an integer number of half wavelengths, but the improvement is even bigger if so is done. The optimal top mirror reflectance is quite low, somewhere around 10-20 %. However, the emission from the long resonant cavity will be split into several peaks at different wavelengths, and these wavelengths will be different depending on what angle you look at the LED from. This might be unwanted behavoiur for some applications.

6.2 Conclusions of the measurements

We see that the grid-shaped electrodes output more light power, with type D being the best, followed by type C, B and the non-grid, dot-shaped A as the worst. Output is also improved by the SiN current blocking layer, improving the green type B electrodes by 33 %. For the dot-shaped type A electrode, the output is improved by smaller contacts. None of these things affect the spectral properties. The best electrode thus would probably be a a type D with a current blocking layer under a bond pad that is as small as possible while also being practical to wire bond to. The measurement results differ between wafer pieces and chip, in both output power and electronic properties. While this means that the absolute values wont be the true values for the packaged end product, the different electrodes ought to be affected the same way, making comparisons possible.

6.3 Further work

Measurements need to be done on packaged LEDs as well, to check if the results stand. A RCLED based on the investigated structures could be realized, but if the emission needs to be in a single spectral peak, and/or the emission pattern needs to be in one straight ahead lobe, the structure needs to be shortened.

Otherwise other light extraction schemes might be considered. Either way, more simulations would be needed.

Bibliography

[1] E. Fred Schubert, *Light Emitting Diodes 2nd edition*, Cambridge university press, 2006

[2] Dana Delbeke, Ronny Bockstaele, Peter Bienstman, Roel Baets, and Henri Benisty, *High-Efficiency Semiconductor Resonant-Cavity Light-Emitting Diodes: A Review*, IEEE JOURNAL ON SELECTED TOPICS IN QUANTUM ELECTRONICS, VOL. 8, NO. 2, MARCH/APRIL 2002

[3] Miles V. Klein, Thomas E. Furtak, *Optics 2nd edition*, John Wiley & Sons, Inc, 1986

[4] C J R Sheppard, *Approximate calculation of the reflection coefficient from a stratified medium* Pure Appl. Opt. 4 (1995) 665-669

[5] Eugene Hecht, *Optics 2nd edition* Addison-Wesley Publishing Company 1987

[6] M.R. Krames, M. Ochiai-Holcomb, G.E. Hfler, C. Carter-Coman, E.I. Chen, I.-H. Tan, P. Grillot, N.F. Gardner, H.C. Chui, J.-W. Huang, S.A. Stockman, F.A. Kish, M.G. Craford, T.S. Tan, C.P. Kocot, M. Hueschen, J.Posselt, B. Loh, G. Sasser, and D. Collins, *High-power truncated-inverted-pyramid* $(Al_xGa_{1-x})_{0.5}In_{0.5}P/GaP$ *light-emitting diodes exhibiting >50 % external quantum efficiency*, APPLIED PHYSICS LETTERS VOLUME 75, NUMBER 16 18 OCTOBER 1999

[7] Michael R Krames, Fred A Kish, Jr., Tun S Tan, *Light extraction from a semiconductor light-emitting device via chip shaping*, US Patent 6,229,160 B1 2001

[8] Po-Hsun Lei, Ming-Jun Ding, Yuan-Chih Lee, Meng-Jung Chung, *Textured zinc oxide prepared by liquid phase deposition (LPD) method and its application in improvement of extraction efficiency for 650nm resonant-cavity light-emitting diode (RCLED)*, Journal of Alloys and Compounds 509 (2011) 61526157

[9] T. Fujii, Y. Gao, R. Sharma, E. L. Hu, S. P. DenBaars, and S. Nakamura, *Increase in the extraction efficiency of GaN-based light-emitting diodes via surface roughening*, APPLIED PHYSICS LETTERS VOLUME 84, NUMBER 6 9 FEBRUARY 2004

[10] B.J. Kim, H. Jung, J. Shin, M.A. Mastro, C.R. Eddy Jr., J.K. Hite, S.H. Kim, J. Bang , J. Kim, *Enhancement of light extraction efficiency of ultraviolet light emitting diodes by patterning of SiO2 nanosphere arrays* Thin Solid Films 517 (2009) 27422744

[11] R. Windisch, C. Rooman, S. Meinlschmidt, P. Kiesel, D. Zipperer, G. H. Dhler, B. Dutta, M. Kuijk, G. Borghs, & P. Heremans *Impact of texture-enhanced transmission on high-efficiency surface-textured light emitting diodes*, Applied Physics Letters 79, 2315 (2001)

[12] E.F. Schubert, Y.-H. Wang, A. Y. Cho, L.-W. Tu and G.J. Zydzik, *Resonant cavity light-emitting diode*, Appl. Phys. Lett., Vol. 60, No. 8 25 February 1992

[13] Ray-Hua Horng, Wei-Kai Wang, Shin-Yung Huang, Dong-Sing Wuu, *Effect of Resonant Cavity in Wafer-Bonded Green InGaN LED With Dielectric and Silver Mirrors*, IEEE PHOTONICS TECHNOLOGY LETTERS, VOL. 18, NO. 3, FEBRUARY 1, 2006

[14] http://www.crosslight.com/

[15] www.refractiveindex.info, accessed July 2013

[16] Jung-Tang CHU, Chih-Chiang KAO, Hung-Wen HUANG, Wen-Deng LIANG, Chen-Fu CHU, Tien-Chang LU, Hao-Chung KUO and Shing-Chung WANG, *Effects of Different n-Electrode Patterns on Optical Characteristics of Large-Area p-Side-Down InGaN Light-Emitting Diodes, Fabricated by Laser Lift-Off* Japanese Journal of Applied Physics Vol. 44, No. 11, 2005, pp. 79107912

[17] S.H. Tu, J.C. Chen, F.S. Hwuc, G.J. Sheu, F.L. Lin, S.Y. Kuo, J.Y. Chang, C.C. Lee, *Characteristics of current distribution by designed electrode patterns for high power ThinGaN LED*, Solid-State Electronics 54 (2010) 14381443